T.2: LIBS: A laser based tool for elemental analysis of materials

Sunita Ahlawat*, Diksha Garg, B. N. Upadhyaya, and P. K. Mukhopadhyay

Advanced Laser Development & Applications Division, RRCAT
**E-mail: rsunita@rrcat.gov.in*

Abstract

Laser-Induced Breakdown Spectroscopy (LIBS) is a versatile technique used for elemental analysis. It works by focusing a high-energy pulsed laser on a sample surface to create a tiny plasma, and the spectral analysis of light emitted from this plasma provides information about the elements present in the material. LIBS can detect almost all elements in the periodic table, including low atomic number (low-Z) elements, and requires a little to no sample preparation. It enables rapid, real-time analysis and also allows stand-off measurements from several meters away. The technique is quasi-non-destructive, as it removes only a very small amount of material (~100's of micron), and it can be used for solids, liquids, and gases under ambient, vacuum, or controlled environments. In addition, LIBS systems can be made portable and used with fiber-optic probes, making them suitable for field applications. In ALDAD, RRCAT, several LIBS setups have been developed, each suitable for specific applications including in-situ measurements, stand-off analysis over several meters, and for use in difficult-to-access or hazardous environments. In this theme article, an overview of the various LIBS systems and analysis approaches for material characterization developed at RRCAT, has been presented.

1. Introduction

Laser-Induced Breakdown Spectroscopy is an optical emission spectroscopy technique that enables direct elemental analysis of samples through spectroscopic analysis of laser induced plasma. In this technique, an energetic pulsed laser is focused on a sample surface, producing irradiance of the order of 10^{10}-10^{11} W/cm^2. When this irradiance exceeds the breakdown threshold of the sample material, the rapidly deposited energy leads to intense localized heating, causing melting and vaporization of the surface, followed by ionization of the ablated vapor. This results in formation of a transient plasma composed of atoms, ions, electrons, and clusters. The plasma is very hot in the beginning and emits broadband light called continuum. As the plasma cools down, distinct atomic and ionic spectral lines begin to appear in the plasma emitted light. The spectroscopic analysis of this radiation provides elemental information about the sample.

Although the early demonstrations of LIBS dates back to 1960s [1], soon after the invention of laser, but its initial applications mainly utilized the plasma as a source for spark-based methods. Interest in LIBS was revived in the 1980s with advancements in laser and spectroscopic technologies. However, still the laser and spectrometer systems used in early LIBS systems were bulky and suitable for laboratory applications. In addition to hardware limitations, difficulties in handling and interpreting the LIBS data, which is often huge and complex, made LIBS analysis challenging and limited its wider use. Recent technological advancements have led to the development of compact and efficient flash lamp pumped lasers. Further, alternate laser sources such as diode-pumped solid-state (DPSS) lasers, fiber lasers, and microchip lasers, which require less cooling, consume less power, and reduce overall LIBS system size, are also being explored. Similarly, improvements in spectrometers have made it possible to use compact single or multi-channel Czerny–Turner spectrometers that can detect the required wavelength range with sufficient resolution. In addition, the use of machine learning techniques has made it easier to analyse complex LIBS data, enabling faster and more reliable results. All these technological advancements have transformed LIBS from a laboratory-based technique into a robust and portable tool suitable for field use.

When compared to other conventional elemental analysis techniques, LIBS offers several advantages. For example, inductively coupled plasma optical emission spectroscopy (ICP-OES) usually requires extensive sample preparation, such as digestion and dilution, and is a bulky laboratory instrument, making it difficult to use in the field. Similarly, X-ray fluorescence (XRF) has poor sensitivity for low atomic number elements. Further, both techniques generally require the sample to be placed close to the instrument and cannot perform analysis of remotely placed samples. In contrast, LIBS requires minimal or no sample preparation, and can detect almost all periodic table elements, including low atomic number elements. It can also perform remote (stand-off) measurements over distances of several meters, allowing its use in harsh or hazardous environments and making it highly suitable for field applications. These advantages have enabled LIBS applications across diverse fields, including environmental monitoring of heavy metals and trace elements, geological and planetary exploration for elemental characterization, and industrial process monitoring for alloy identification and quality control [2]. More recently, it has gained attention in nuclear field for fuel characterization and radioactive waste analysis[3].

In this article, we will first outline the basic working principle of LIBS, including plasma generation and spectral emission processes. We will then present an overview of the different LIBS systems developed at RRCAT and the analytical approaches used for elemental analysis, highlighting their capabilities and application areas.

2. Basics of LIBS

When a high energy laser pulse is focused onto a material surface, the initial interaction begins with absorption of laser energy by free electrons present in the material. In this process, free electrons absorb photons from the laser field while undergoing collisions with ions or neutral atoms via a process known as Inverse Bremsstrahlung (IB). These energetic electrons then transfer their energy to the lattice, resulting in rapid lattice heating within the irradiated region. As the lattice temperature increases, the material begins to undergo phase transitions, first reaching the melting point, and forming a thin molten layer at the surface. When the rate of energy deposition exceeds the rate with which energy can be dissipated through thermal conduction and evaporation, deeper layers of the material may also melt. Under sufficiently rapid heating, the temperature of the superheated liquid can approach the critical temperature, resulting in phase explosion. In this process, the molten material undergoes an explosive transition into a mixture of vapour and fine droplets, ejecting atoms, ions, clusters, and free electrons that form a plasma plume. Since the plasma consists of atoms and ions ejected from the sample, therefore, it carries information about the sample's elemental composition.

Such conditions of rapid energy deposition, are typically achieved with nanosecond or shorter (picosecond/ femtosecond) laser pulses. Among these, nanosecond lasers are most commonly preferred in LIBS due to their simpler design, lower cost, and ability to generate sufficient plasma emission for reliable detection compared to picosecond and femtosecond laser systems. For longer pulse durations (e.g., microsecond), the rate of heat deposition is lower and can be balanced by thermal diffusion and evaporation. In this case, material removal occurs primarily through thermal evaporation, which may result in elemental fractionation due to differential vaporization of elements and thus reducing the possibility of producing a stoichiometric plasma plume. As a result, accurate composition analysis becomes difficult.

The mechanisms of laser energy absorption and subsequent plasma formation vary significantly depending on the type of material. In metals, there is already a sea of free electrons present to absorb the laser radiation. However, in case of semi-conductors, the laser energy is initially absorbed by conduction electrons which then undergo impact ionization, leading to avalanche multiplication and formation of large free electrons. In insulators, the initial seed electron may be provided by some impurities or field enhancement at defects or multi-photon ionization. Eventually, all materials start behaving optically like metals leading to plasma formation. However, the laser breakdown threshold differs for metals, semiconductors, and insulators, mainly due to differences in initial carrier density and band structure.

The laser induced plasma is initially very hot and dense, with temperatures of the order of ~10,000 K and electron densities around ~10^{17} cm^{-3}. At this early stage, the emission is dominated by continuum radiation arising mainly from free-free (Bremsstrahlung) and free-bound (radiative recombination) transitions. Free-free transition occurs when energetic electrons are decelerated in the Coulomb field of ions, while free-bound emission results from recombination of free electrons with ions. These processes produce a strong broadband emission known as continuum emission, which does not consist of any element specific information and hence is of no use from elemental analysis point of view. Once the laser pulse has ended, the plasma expands rapidly and generates a shock wave. As plasma expands and cools, its temperature and electron density decreases, causing excited atoms and ions to relax to lower energy states and emit characteristic spectral lines. This line emission is used for elemental analysis in LIBS. The entire process of nanosecond laser material interaction and plasma emission is shown schematically in Figure T.2.1.

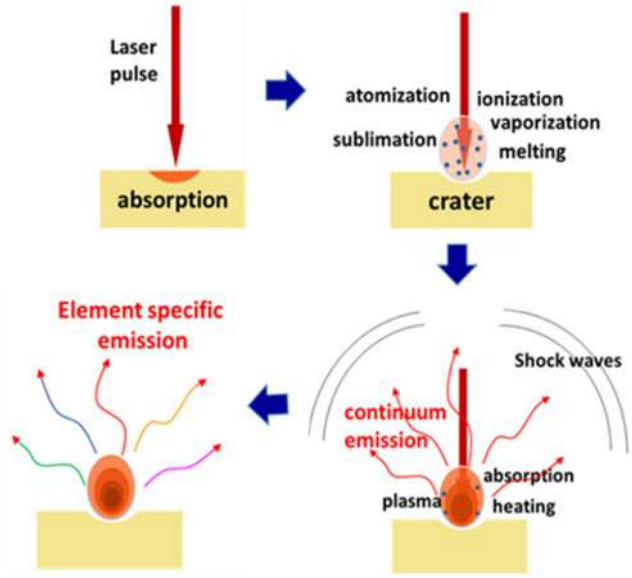

Fig. T.2.1: A schematic showing absorption of a nanosecond laser pulse in a material, leading to plasma formation, and continuum light emission followed by characteristic or element specific light emission.

The initial plasma emission is dominated by strong continuum radiation that can obscure characteristic spectral lines, and therefore, is not desired. To overcome this, time-gated detection is used, where the detector is triggered after a short delay of a few μs, allowing for the continuum to decay and the characteristic spectral lines to become prominent. A schematic of the time evolution of plasma emission is shown in Figure T.2.2.

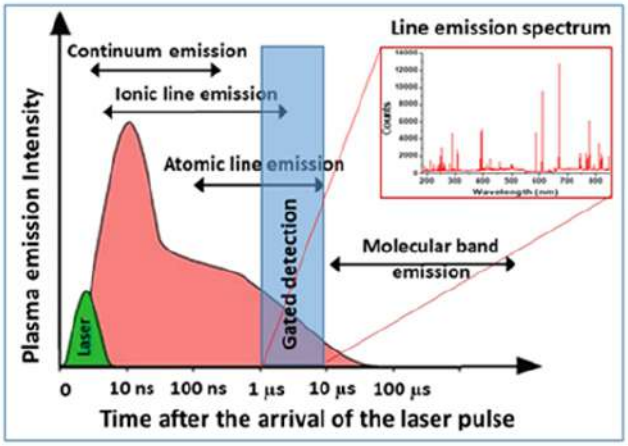

Fig. T.2.2: A schematic showing time evolution of plasma emission produced by a nanosecond pulse. Inset shows the LIBS spectrum of a soil sample recorded 1 µs after the laser pulse, where the nearly flat background indicates that continuum emission has largely decayed.

At further later stages of plasma evolution, i.e., several 10's of microsecond, the plasma temperature becomes even lower and recombination processes occur, where molecular species may form through recombination of ablated atoms or interaction with the surrounding atmosphere. This can lead to the appearance of molecular band emissions, e.g., CN, C_2, AlO, CaO, which appear as band structures and can provide additional information about the sample.

Although LIBS offers many advantages, several issues make the interpretation of its spectral data quite complex. One major issue is strong matrix effects, where variations in the composition and physical properties of the sample influence the laser matter interaction and consequently, the plasma temperature and emission. As a result, even for the same concentration of an element, the emitted intensity can vary from one matrix to another. This leads to poor transferability of calibration models across different sample types. The second important issue is self-absorption, a phenomenon in which photons emitted by the excited atoms or ions within the plasma are reabsorbed by the same species in lower energy states. This occurs when the radiation emitted by the hotter inner regions of the plasma gets reabsorbed by the outer colder layers, which contains a higher population of ground-state or low energy atoms or ions. This effect is more pronounced for strong resonance lines of major elements. As a result, the emitted line intensity does not increase proportionally with concentration, leading to reduced line intensity, distorted peak shapes, and deviation from linear calibration behaviour. Further, different spectral lines of the same species undergo different degree of self-absorption making the analysis further challenging. Another important factor which affects the LIBS signal is shot-to-shot fluctuation, where the spectral signal varies significantly between successive laser pulses. This variation arises from small changes in laser energy, beam profile, and sample surface conditions, which affect plasma formation and hence the emission intensity. In addition, spectral interference and overlapping emission lines make it difficult to identify and quantify elements in complex samples. All these factors collectively make the spectral interpretation challenging and necessitates the use of advanced data analysis techniques.

3. Analysis techniques

The analysis of LIBS spectra can be broadly categorized into qualitative and quantitative analysis. In qualitative analysis, the primary objective is to identify the elements present in the sample. This is achieved by matching the observed spectral lines with known atomic or ionic emission lines available in standard spectral databases such as those provided by National Institute of Standards and Technology (NIST)[4]. Each element emits radiation at characteristic wavelengths corresponding to electronic transitions between energy levels. By comparing the measured wavelengths with reference values, the presence of specific elements in the sample can be confirmed.

Quantitative analysis is commonly performed using calibration-based methods, where the intensity of selected emission lines is correlated with known concentrations of reference standards to generate calibration curves. However, the univariate calibration, which is based on analysis of single spectral line, is often limited by factors known to complicate the LIBS analysis, i.e., matrix effects, self-absorption, plasma fluctuations, and spectral line overlap, etc. These factors can alter line intensities and lead to a non-linear relationship between spectral intensity and elemental concentration, making it difficult to perform reliable analysis on the basis of individual spectral lines. To overcome these challenges, multivariate approaches, including machine learning (ML) techniques such as principal component analysis (PCA), random forest (RF), support vector machines (SVM), and artificial neural networks (ANN), are increasingly being employed. Unlike univariate methods, which rely on an individual spectral line, ML approaches utilize information from a large number of spectral lines or entire spectrum simultaneously, allowing them to capture subtle correlations and complex patterns within the data. Methods such as PCA reduce data dimensionality by transforming the original high-dimensional spectral data into a smaller set of principal components that capture most of the variance in the dataset. PCA not only helps in noise reduction and feature extraction but also allows to visualize underlying patterns, trends, and clustering of samples leading to better understanding of similarities or differences within the dataset. ML models such as RF, SVM, and ANN can model complex, non-linear relationships among multiple spectral features and can be applied to LIBS data for classification or quantitative analysis. RF works by building an ensemble of decision trees, each of which learns a series of rules from the training data to

make predictions. Randomness is introduced during tree construction to ensure diversity, improve accuracy, and reduce overfitting. SVM works by finding the best hyperplane to separate classes in the data, maximizing the margin between them. It can use kernel functions to handle non-linear separation, making it effective for classifying samples with overlapping or subtle spectral differences. ANN emulate the structure and function of the human brain, consisting of interconnected layers of artificial neurons. Each neuron receives inputs, applies weights and a bias, and passes the result through an activation function to produce an output. By adjusting these weights during training, the network learns complex patterns and relationships in the data, enabling it to make accurate predictions or classifications. Thus, ML techniques can handle the complex LIBS data and provide fast and reliable elemental analysis.

4. LIBS configurations: A general overview

LIBS offers high versatility in configuration, allowing systems to be customized according to specific sample requirements and operational environments. For example, laboratory-based LIBS systems are typically designed for high sensitivity and spectral resolution, often incorporating high energy nanosecond Nd:YAG lasers, free-space beam delivery optics, and high-resolution spectrometers coupled with intensified detectors such as intensified charge coupled devices (ICCDs) for time-resolved measurements. LIBS setups based on picosecond or femtosecond lasers produces reduced thermal effects and improved spatial resolution[5]. Industrial and field-deployable LIBS systems require compactness and robustness, and therefore prefer compact laser systems, fiber-optic beam delivery and compact spectrometers [6]. Other more advanced LIBS systems include, double-pulse lasers for enhancing plasma characteristics and improving analytical performance [7], imaging and micro-LIBS for spatial mapping [8].

5. LIBS setups developed at RRCAT and their analytical performance

5.1 Benchtop LIBS setup: A benchtop LIBS setup (Fig. T.2.3) was developed using a flash lamp pumped 1064 nm Nd:YAG laser, with energy up to 150 mJ, pulse duration of ~ 6 ns and repetition rate of 10 Hz for plasma generation. The laser energy at the sample was controlled via a combination of a half wave plate and polarizer. The laser beam was focused over the sample surface using a 100 mm focal length lens. The samples were placed over a manual XYZ stage. The plasma emission was collected using a 10 mm focal length lens and coupled into a fibre. The other end of the fibre was coupled to a five-channel spectrometer. The spectrometer has a spectral range of 200–815 nm and resolution varying from 0.1 nm at lower wavelengths to 0.18 nm at longer wavelengths. The spectrometer software was used to trigger the laser pulse firing as well as to adjust the delay time after laser pulse to start spectrum acquisition. The delay time was set at 1 μs, as by this time most of the continuum background was found to get extinguished and the LIBS line spectra could be recorded with a good signal to noise ratio.

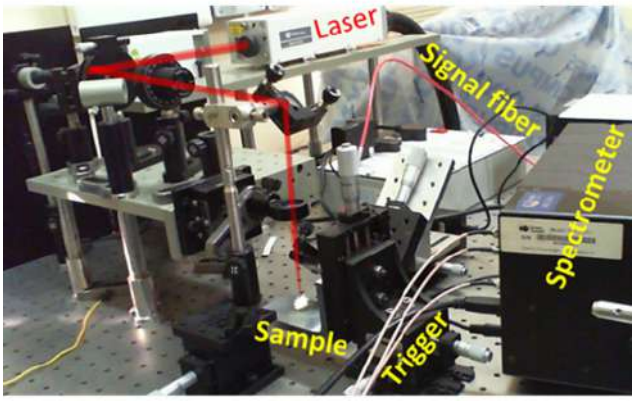

Fig. T.2.3: A view of the benchtop LIBS experimental setup.

5.1.1. Quantitative analysis of water-based samples: This setup was used to perform analysis of heavy element in water samples– [9]. One of the easiest methods to analyse liquid sample using LIBS is to solidify over some solid substrate. However, the main issue with this approach is the non-uniform deposition of solute particles over the substrate, due to the well-known coffee ring effect [10], which affects the repeatability of the LIBS spectra collected from different area of the solidified sample. To overcome such problem, we developed a laser textured silicon substrate. For laser texturing, an in-house built DPSS laser at 532 nm having nanosecond pulse duration was used [11]. The laser texturing imparted superhydrophilicity to the silicon surfaces, which resulted in uniform spreading and solidification of the water-based samples over the textured area. Although metals like steel, aluminium, and copper also become superhydrophilic after laser texturing but silicon was chosen for its stable superhydrophilic nature. The laser textured superhydrophilic metals start transitioning towards hydrophobicity soon after laser texturing due to the high reactivity of the metal oxides, formed during laser texturing, with ambient gases. In contrast, silicon does not react with ambient gases and remained superhydrophilic for a few months, and hence can be stored for later use.

To evaluate the uniformity of sample deposition over the laser textured area, a two-dimensional (2-D) LIBS scan was performed over the textured area at a step size of 0.5 mm in both the directions. Figure T.2.4(a) shows a laser textured silicon sample after it has been scanned by the LIBS DPSS laser. Uniformity of the samples solidified upon evaporation of water was determined by using the shot-to-shot relative

standard deviation (RSD) of the LIBS spectra recorded from the central region of the textured area. The RSD for the solidified water samples containing Cr, Cd and Sr was found to be in the range of ~ 6.4–7.8% (Fig. T.2.4(b)) and that for the blank laser textured silicon, i.e., without any sample, was found to be ~ 4.5%. These results suggested that the water-based samples got solidified with good uniformity within the central region of the superhydrophilic textured area.

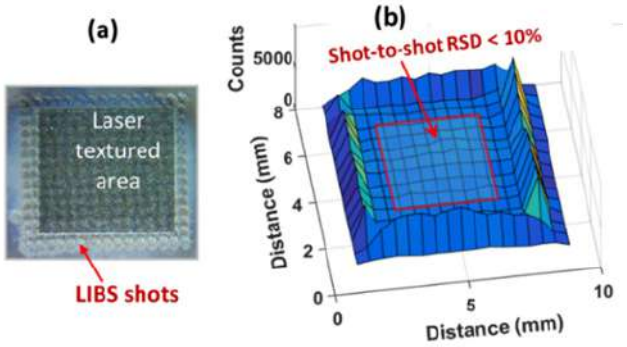

Fig. T.2.4: (a) A view of a laser textured silicon sample after it has been scanned by the LIBS laser and (b) 2-D LIBS scan for the Cr line at 425.44 nm over the laser textured area after 3 µL droplet of 10 ppm Cr solution was solidified.

The laser-textured area also helped in confining the liquid samples within the structured region due to its superhydrophilic properties. As a result of this confinement, even a small liquid volume of about 3 µL was sufficient to achieve ppm or sub-ppm level limits of detection (LOD), depending on the sensitivity of the selected LIBS spectral line. Furthermore, the LOD could be improved to ppb level by repeating the process of placing and drying small droplets over the textured area without significantly affecting the shot-to-shot RSD of LIBS spectral peaks for up to a few 100's of such repetitions. Table T.2.1 presents the LOD values obtained with different sample volumes for Cr, Sr and Cd.

Table T.2.1. Limit of detection (LOD) obtained for different elements with different volumes.

Element	Volume	LOD
Cr	3 µL	1.1 ppm
Cr	30 µL	0.41 ppm
Cr	100 µL	83.9 ppb
Cr	500 µL	14.9 ppb
Cd	3 µL	5.2 ppm
Cd	500 µL	16.8 ppb
Sr	3 µL	0.15 ppm
Sr	500 µL	13.4 ppb

5.1.2 Classification of steel samples

Steel grade identification is important in industrial quality control as well as efficient sorting of scrap during recycling processes. Considering the capability of LIBS for rapid, in-situ, and multi-element analysis with minimal sample preparation, we explored its use for steel grade identification [12]. Figure T.2.5 shows LIBS spectrum of a steel grade AISI 316. It can be noted that the spectrum is highly crowded due to the presence of multiple alloying elements, with major elements such as Fe, Cr, and Ni producing a large number of closely spaced spectral lines. This high line density leads to significant spectral overlap and interference, making it difficult to resolve individual element contributions. The challenge becomes even more pronounced when trying to distinguish between steel grades, which differ mainly in the concentrations of minor alloying elements. These subtle differences get masked by the dominant lines of major elements and by variations in plasma conditions, surface inhomogeneities, and shot-to-shot fluctuations. Therefore, ML techniques were employed for steel grade classification.

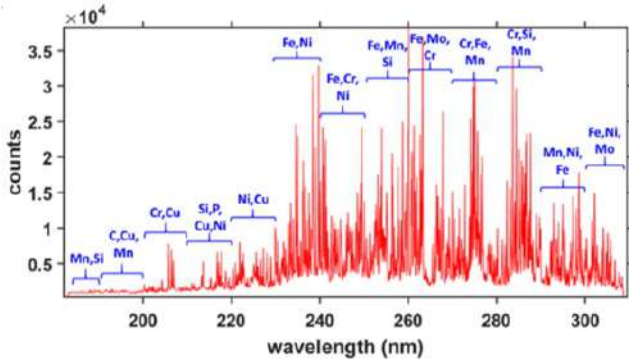

Fig. T.2.5: LIBS spectrum of steel grade 316 sample in the range of 185 nm to 310 nm.

When applying machine learning (ML) to LIBS data, proper pre-processing is essential. An important pre-processing step is feature scaling, e.g., min–max or standard scaling, which is done to bring all the spectral features to a comparable scale and avoid bias from highly intense peaks. In min-max (MM) scaler, each spectral feature x is normalized within a fixed scale using the formula $(x\text{-}x_{min})/(x_{max}\text{-}x_{min})$; and in standard scaler (SS), features are scaled using $(x\text{-}x_{mean})/x_{std}$. Here, x_{min}, x_{max}, x_{mean} and x_{std} are maximum, minimum, mean and standard deviation value of a feature x determined over all the spectra. In spectroscopy, another type of normalization is commonly practiced and this is called spectrum normalization (commonly area normalization). This is done to bring all the spectra to a common scale and thus compensating for the overall changes in spectral intensity among different spectra. For area normalization (AN), each spectrum is divided by total area under the spectrum. We combined both the normalization techniques and found that classification accuracy of ML techniques improved considerably. For this study, a total of 11 steel samples belonging to seven grades: 304, 304L, 316, 316L, 410, 4140 and 440, were used. Figure T.2.6 shows the results of SVM based classification of the

samples into their respective grades. The grade prediction accuracy was highest when area normalization was followed by min-max feature scaling. The improved accuracy can be attributed to the complementary nature of the two normalization steps. In a data set consisting of multiple spectra arranged in different rows: area normalization operates row-wise reducing the effect of shot-to-shot fluctuations, while feature scaling operates column-wise, ensuring uniform contribution of all spectral features across multiple spectra. The grade identification accuracy with area normalization followed by min-max scaler was found to be 98.9%. It may be noted here that some of the grades to be identified were quite similar, e.g., 304 and 304L, which mainly differ in the concentration of carbon, which is present in quantity less than 0.08%. The high classification accuracy suggested that LIBS can be used for reliable grade classification of steel samples.

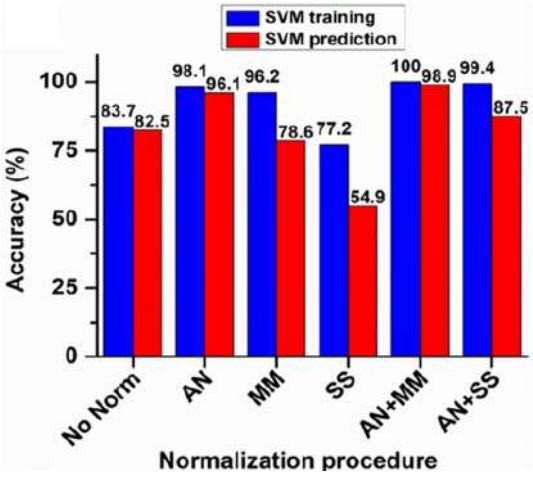

Fig. T.2.6: Classification accuracy of different steel grades during training of SVM models as well as for prediction made using the trained SVM models, when different normalization procedures were applied. AN: area normalization, MM: min-max scaler, SS: standard scaler.

5.2 Trolley mounted stand-off LIBS setup

In many practical scenarios, samples may be located in hazardous environments or at inaccessible locations, where direct contact or close-range analysis is not feasible. For such applications, stand-off LIBS provides an effective solution by enabling analysis of materials from a distance without the need for sample handling. We have developed a stand-off LIBS setup using a nanosecond pulse laser of 350 mJ pulse energy [13]. To focus the laser beam tightly up to several meter distances, it was first expanded by 4X using a combination of a plano-concave lens of −25 mm focal length and a plano-convex lens of 100 mm focal length. Laser focusing distance was changed by adjusting distance between the two lenses. For efficient collection of signal from such long distances, a 4″ Maksutov–Cassegrain telescope was used. The collected signal was coupled to a multi-channel Czerny Turner spectrometer via an optical fiber. The entire setup was mounted on a wheeled trolley and is capable of analysing the samples from a distance of ~10 m (Fig. T.2.7). Using the setup, investigation was performed on detection of Sr, which may be present as a radioactive contamination in nuclear reactors on stainless steel. For the study, residual

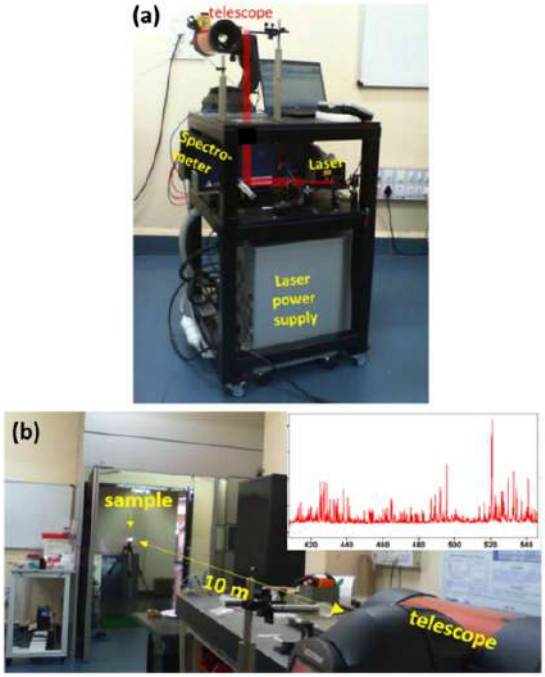

Fig . T.2.7 (a): A view of the trolley mounted stand-off LIBS setup and (b) a photograph showing working of the stand-off LIBS setup for steel sample located at a distance of 10 m away. Inset shows the spectrum recorded from the sample.

dried spots left behind by 1 µL droplets of Sr solution were analyzed using LIBS from a distance of 6 m. Figure T.2.8(a) indicates the spectral features of Sr in the crowded steel spectrum, while Figure T.2.8(b) indicates the location of the LIBS shot fired over the dried Sr solution droplet. A calibration curve was prepared for intensity of Sr peaks at different concentrations of Sr (Fig. T.2.8(c)). From this calibration curve, the limit of detection of Sr was estimated to be ~ 30 ppb, which is equivalent to ~ 1.5 ng/cm^2.

5.3. LIBS setup based on low energy high repetition rate DPSS laser

Both benchtop LIBS and stand-off LIBS setups were developed using a flash lamp pumped Nd:YAG laser with pulse energy in range of 150 mJ -350 mJ. This pulse energy is high enough to cause breakdown of the material and form a strong plasma signal using a single pulse. We observed that a weak plasma could also be formed by focusing in-house built DPSS Nd:YAG laser system with pulse energy of up to 2 mJ and repetition rates up to 80 kHz, on metallic samples.

Therefore, we explored the use of this laser system for LIBS— [14]. This system offers advantages such as requirements of reduced thermal management and longer operational lifetime. Further, due to the low pulse energy, the generated plasma and associated continuum emission was negligible, which allowed trigger-free spectral acquisition. This is an additional advantage as there is now no need for synchronization of spectrometer with laser. The plasma signal is also weak due to the low pulse energy, but by accumulating

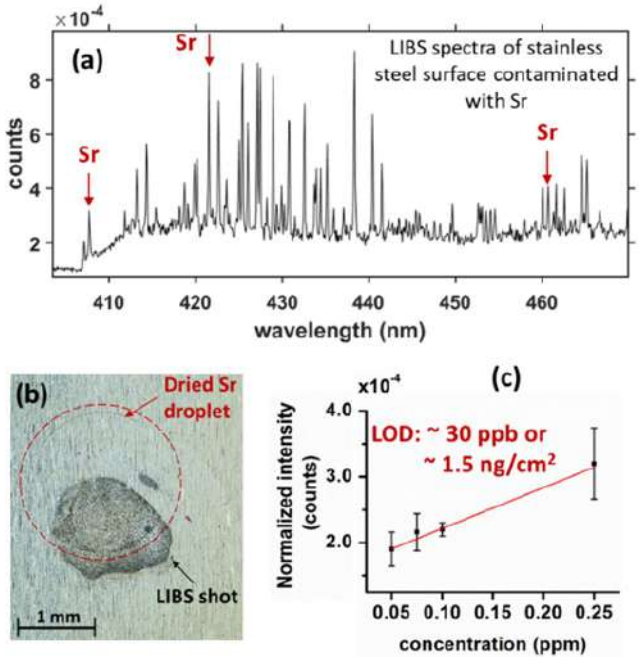

Fig. T.2.8: (a) LIBS spectra recorded from a distance of 6 m from the spot left behind by evaporation of Sr solution droplet on steel substrate, (b) image of the dried Sr droplet (dotted circle) along with the LIBS shot mark and (c) calibration curve prepared using Sr peak at ~ 421.5 nm.

signal over a large number of pulses, a good signal-to-noise ratio can be recorded. While this approach relaxes the need of synchronization, the high repetition rate of the laser introduces a new requirement of sample scanning. Due to kHz repetition rate of the laser, the laser pulses form a deep crater on the sample if allowed to hit at the same sample site during spectral acquisition. These deep craters disturb the laser focusing and hence weaken the laser matter interaction and the plasma intensity. Therefore, in this setup, the sample was mounted on a motorized XY stage and continuously moved during analysis to ensure deep craters are not formed. Figure T.2.9 shows a view of the experimental setup using the DPSS laser. By optimizing the experimental parameters like pulse energy, laser repetition rate and sample scanning velocity, LIBS spectra could be recorded with inter-spectrum variability similar to that obtained for conventional high pulse energy LIBS.

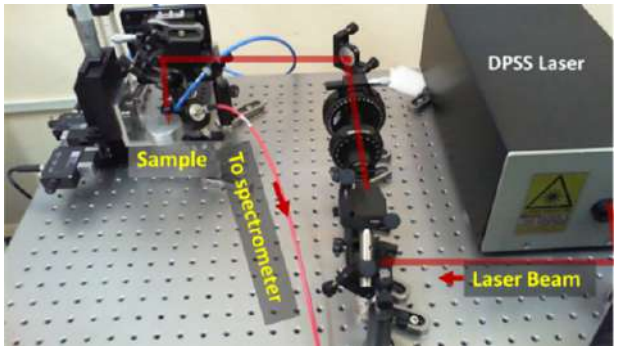

Fig. T.2.9: A view of the LIBS setup developed using the in-house built DPSS laser with 2 mJ of maximum pulse energy and 80 kHz of maximum repetition rate.

Analytical performance of this set up was evaluated by performing quantitative estimation of steel alloying elements. For the quantitative analysis, 19 steel samples were analyzed and ~1000 spectra were recorded from each sample. Figure T.2.10 shows LIBS spectra recorded from various steel grades, which look quite similar because of compositional similarity.

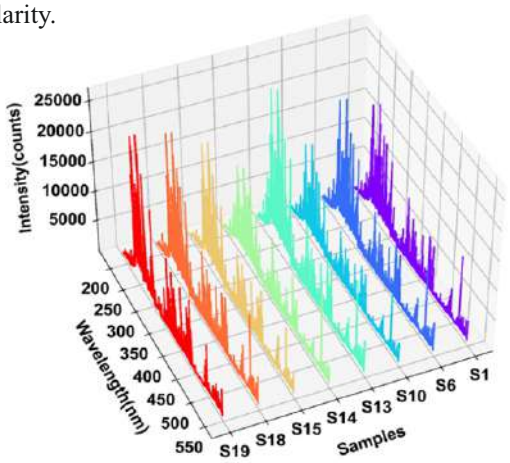

Fig. T.2.10: LIBS spectra of different steel samples recorded using DPSS laser-based LIBS setup.

The concentration of the various steel alloying elements was first determined using other methods like ICP-OES or Spark-OES and these values were used as reference standards for calibration. As an initial approach, a simple univariate (single spectral line) calibration method was employed by correlating the intensity of individual spectral peaks with increasing elemental concentration. However, the data points exhibited significant scatter, indicating poor correlation between the intensity and concentration. Therefore, the calibration curves derived from this method led to large prediction errors, with relative mean errors ranging from ~ 5% to 450% for different elements. The observed scattering of data points in univariate analysis is expected to be due to the factors such as self-absorption effect, matrix effect, etc., which make the LIBS spectra complex. Since single peak

analysis did not perform satisfactorily, a machine learning approach based on the random forest algorithm was employed. During training, the model learns the optimal patterns in the data, which are then applied to new data for prediction. To improve robustness and reduce overfitting, randomness is introduced during tree construction, and the final prediction is obtained by aggregating the outputs of all trees. Figure T.2.11 shows the results of random forest regression for various steel elements, where 15 steel samples were used to train or calibrate the RF regression models. Thereafter, these RF models were used to predict the concentration of elements of 4 steel samples. The results of prediction are also presented in the figure. Table T.2.2 shows the tested range of elemental concentration, observed relative error (RME) between the actual concentration values and predicted concentration values. The benchmark range of RME obtained in LIBS for different range of elemental concentration are also listed in the Table, which suggests that the RME values are well within the benchmark range.

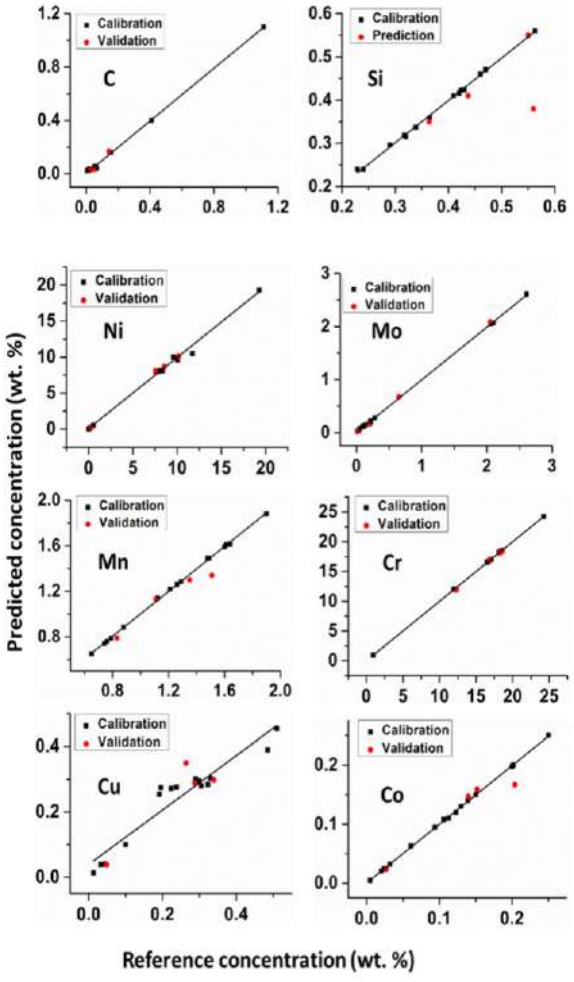

Fig. T.2.11: Random forest regression predicted values versus references values of concentrations of various elements for the calibration and validation of samples.

Table T.2.2. Relative mean error in predicted concentrations of various steel elements using random forest regression.

Element	Tested concentration range	Observed relative mean error (RME)	Benchmark RME range
Cr	12.32 – 18.38%	1.41 %	1-5 % (for element conc. >1%)
Ni	0.25-10.15%	2.08 %	
Mo	0.029-2.05%	5.45 %	
Mn	0.83-1.51%	5.40 %	
Si	0.36-0.56%	10.78 %	5-20% (for element conc. <1%)
C	0.026-0.14%	11.1 %	
Cu	0.05-0.34%	15.75 %	
Co	0.03-0.2%	9.71 %	

5.4 Fiber optics LIBS setup

As LIBS makes use of laser to obtain the spectra of plasma, therefore offers the possibility to deliver the laser beam through an optical fiber. Further, as the spectra is already being collected using an optical fiber, therefore, the configuration in which both laser delivery and signal collection is done using fibers is referred to as fiber-optic LIBS (FO-LIBS). A schematic of the developed FO-LIBS setup[15] is shown in Figure T.2.12(a). The advantage of this system is that it allows sensitive components of the LIBS setup such as the laser, spectrometer, and detector, to be positioned away from the sample, enabling remote analysis using a fiber-optic probe that incorporates both the laser delivery and signal collection using optical fibers. Figure T.2.12(b) shows a view of the developed FO-LIBS probe. Since FO-LIBS requires the delivery of energetic laser pulses through an optical fiber to generate plasma at the sample surface, a major challenge lies in transmitting these high-energy pulses without causing damage to the fiber itself. Therefore, to reduce the risk of damage, optical fibers of large core diameter of 1000 μm was used for beam delivery. However, such fiber delivery transformed the Gaussian-like input laser beam (Fig. T.2.12 (c)) into flat-top like beam (Fig. T.2.12(d)) due to excitation of multiple modes through the fiber. Figure T.2.12(e) shows the ablation spot formed on a steel sample using the fiber delivered beam.

Even when large core diameter of fiber is used, still to minimize the risk of laser-induced damage, it is preferable to use the lowest pulse energy that is sufficient to generate plasma on the sample surface. It was observed that a pulse energy of as low as 6 mJ (fluence ~1.86 J/cm²) was sufficient to initiate plasma formation on the steel surface. However, the generated plasma could not be sustained over multiple shots as the emission intensity monotonically decreased when multiple pulses were fired at the same sample location and eventually vanished. This behaviour, as shown in Figure

T.2.13(a) was observed for energies up to 10 mJ (fluence ~3.11 J/cm²). Beyond this fluence, the plasma signal was found to be stable and could be sustained over hundreds of shots (Fig. T.2.13(b)).

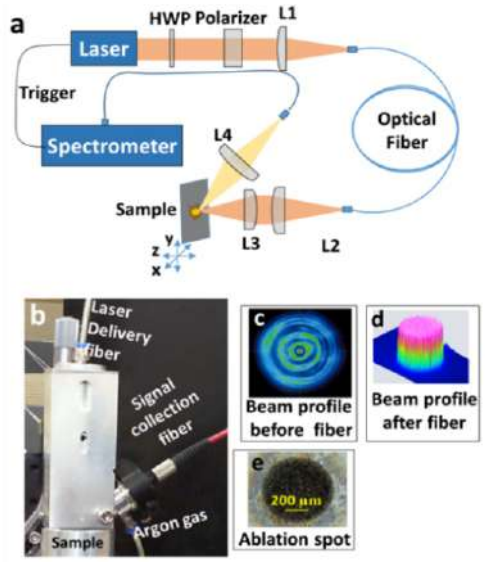

Fig. T.2.12: (a) A schematic of the Fiber-optics LIBS setup, (b) a view of the FO-LIBS probe, (c) laser beam profile before the fiber and (d) after the fiber, and (e) ablation spot formed on steel sample using the fiber delivered beam.

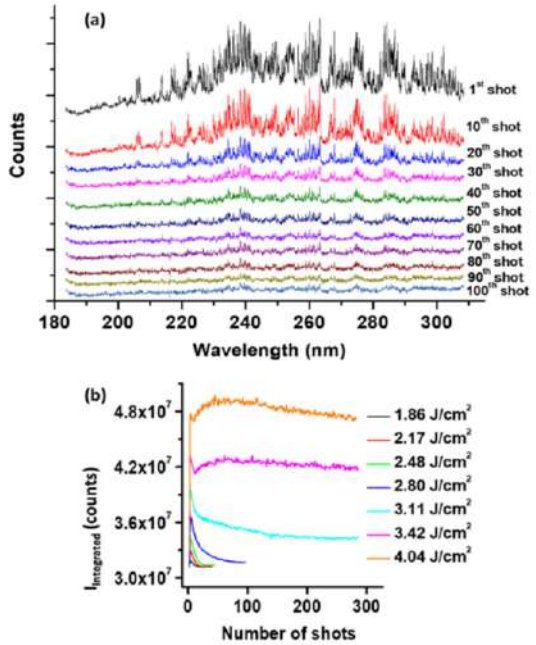

Fig.T.2.13: (a) The plasma spectral signal from a steel sample at a fluence of ~2.8 J/cm² at different laser shot numbers, (b) variation in plasma signal intensity integrated over entire spectra ($I_{Integrated}$) with increasing number of laser shots at various laser fluence.

Further investigations of surface morphology and chemistry indicated that at low fluence, the plasma mainly arises from ablation of the surface oxide layer, which has a lower ablation threshold than the base metal. As this layer is removed with successive shots, the plasma signal diminishes and eventually disappears. A stable and sustained plasma is achieved only when the fluence exceeds the threshold required to ablate the base metal. Unlike free-space LIBS, where a Gaussian beam ensures that some portion remains above the threshold even at low fluence, FO-LIBS produces a top-hat-like beam profile due to multimode fiber propagation. This results in uniform energy distribution, causing the entire spot to be either below or above the threshold, leading to the observed threshold-dependent behaviour.

Since the spectra became stable just above the threshold, quantification was performed at two fluence levels: 4.04 J/cm² (to ensure stable plasma across all samples) and 5.6 J/cm² (well above the threshold). A hybrid machine learning approach was used, with RF for feature selection followed by ANN regression for quantification, offering better accuracy than RF alone and faster performance than ANN alone. A comparison of different error metrics for both fluence values is given in Table T.2.3.

Results presented in Table T.2.3 suggested that there is slight decrease in performance, i.e., increase in the error values for most of the elements at the higher fluence level. This may be due to increase in plasma electron density and hence the associated complexities like self-absorption. Overall, these results suggested that using very high fluence does not prove to be beneficial for the quantitative analysis and using energy values just above the threshold fluence are sufficient to provide accurate quantitative analysis. These results are helpful to optimize the energy requirement of the laser used for FO- LIBS, which is important for development of FO-LIBS systems.

Table T.2.3. Performance metrics of RF-ANN models at two laser fluence values.

	4.04 J/cm ²			**5.6 J/cm ²**		
Element	RME (%)	RMSE (wt. %)	MAE (%)	RME (%)	RMSE (wt. %)	MAE (%)
Cr	1.05	0.199	16.95	1.16	0.213	16.97
Ni	5.61	0.286	22.3	8.10	0.192	13.22
Mo	10.18	0.059	4.4	16.58	0.069	4.49
Mn	3.03	0.041	3.43	3.31	0.044	3.71
C	11.89	0.009	0.68	14.07	0.01	0.81
Si	1.8	0.036	0.83	2.1	0.01	0.92
Cu	7.24	0.059	1.9	8.36	0.032	1.86
Co	7.58	0.015	1.12	8.87	0.02	1.38
P	3.32	0.002	0.11	3.6	0.0018	0.13

Abbreviations: RME: Relative mean error, RMSE: Root mean square error, MAE: Mean absolute error.

6. Future directions

Our future work will focus on making the LIBS systems more efficient, compact, and suitable for real world applications, with fully integrated designs that allow single-window operation of all components and data analysis. We are working to make the DPSS laser-based LIBS system compact and portable for field applications. In fiber-optic LIBS system, we are developing fiber-optics probes, which can analyze samples located several tens of meters away. This will allow their use in confined and harsh environments like hot cells, high-temperature areas, and difficult-to-access industrial locations, where remote and flexible analysis is needed. We also look forward to integrate other analysis techniques like Raman and fluorescence with LIBS to further enhance the scope of applications.

7. Summary

We have developed a range of LIBS systems, including bench-top setup, stand-off system for remote elemental analysis, setup based on low-energy DPSS laser, and fiber-optic LIBS setup. Each of these setup is designed to address specific application requirements. To effectively handle the complex and information-rich LIBS data, we have also developed advanced machine learning approaches that enable reliable qualitative analysis as well as accurate quantitative estimation of elemental composition of samples. Overall, the integration of LIBS hardware with machine leaning data analysis techniques has significantly enhanced the capability of LIBS as an analytical tool. These LIBS systems hold strong potential for applications in environmental monitoring, industrial process control, and remote analysis in hazardous or inaccessible environments.

Acknowledgment

Authors would like to acknowledge the support of Shri Amarjeet Singh and Shri Satish Sahu for providing DPSS laser and Shri Pravin Haedaoo and Shri Bhagwat Prasad for the development of LIBS setups.

References

[1] Brech, F.; Cross, L., Optical Microemission stimulated by a Ruby Maser, Appl. Spectrosc. 16 (1962).

[2] D.A. Cremers, L.J. Radziemski, Handbook of Laser-Induced Breakdown Spectroscopy, Wiley, 2006.

[3] M.Z. Martin, S. Allman, D.J. Brice, R.C. Martin, N.O. Andre, Exploring laser-induced breakdown spectroscopy for nuclear materials analysis and in-situ applications, Spectrochimica Acta Part B: Atomic Spectroscopy 74-75 (2012) 177-183.

[4] NIST LIBS database, (n.d.).

[5] V. Zorba, X. Mao, R.E. Russo, Femtosecond laser induced breakdown spectroscopy of Cu at the micron/sub-micron scale, Spectrochimica Acta Part B: Atomic Spectroscopy 113 (2015) 37-42.

[6] F.J. Fortes, J.J. Laserna, The development of fieldable laser-induced breakdown spectrometer: No limits on the horizon, Spectrochimica Acta Part B: Atomic Spectroscopy 65 (2010) 975-990.

[7] L. St-Onge, M. Sabsabi, P. Cielo, Analysis of solids using laser-induced plasma spectroscopy in double-pulse mode, Spectrochimica Acta Part B: Atomic Spectroscopy 53 (1998) 407-415.

[8] S. Živkovic, A. Botto, B. Campanella, M. Lezzerini, M. Momcilovic, S. Pagnotta, V. Palleschi, F. Poggialini, S. Legnaioli, Laser-Induced Breakdown Spectroscopy elemental mapping of the construction material from the Smederevo Fortress (Republic of Serbia), Spectrochimica Acta Part B: Atomic Spectroscopy 181 (2021) 106219.

[9] S. Ahlawat, P.K. Mukhopadhyay, R. Singh, S.K. Dixit, K.S. Bindra, Laser textured superhydrophilic silicon for uniform solidification and sensitive detection of water-based samples using laser induced breakdown spectroscopy, J. Anal. At. Spectrom. 38 (2023) 883-892.

[10] D. Mampallil, H.B. Eral, A review on suppression and utilization of the coffee-ring effect, Advances in Colloid and Interface Science 252 (2018) 38-54.

[11] S. Ahlawat, A. Singh, P.K. Mukhopadhyay, R. Singh, K.S. Bindra, Nanosecond laser induced glass particle deposition over steel mesh for long-term superhydrophilicity and gravity driven oil water separation, Materials Chemistry and Physics 263 (2021) 124343.

[12] S. Ahlawat, G. Saxena, P. K. Mukhopadhyay, A. Rajan, B. N. Upadhyaya, S. K. Dixit, Two-way normalization of LIBS data for improved machine learning based classification of steel samples, in: NLS-33, Indian Laser Association, Indore, 2025.

[13] S. Ahlawat, P. K. Mukhopadhyay, K.S. Bindra, Demonstration of a Stand-off Laser Induced Breakdown Spectroscopy setup, in: NLS-30, Indian Laser Association, Online, 2022.

[14] S. Ahlawat, A. Singh, S. Sahu, P.K. Mukhopadhyay, R. Arya, S.K. Dixit, Trigger-free LIBS using kHz and a few mJ laser in combination with random forest regression for the quantitative analysis of steel elements, J. Anal. At. Spectrom. 39 (2024) 1927-1937.

[15] S. Ahlawat, D. Garg, P. Tripathi, R.K. Sahu, S. Banik, P.S. Hedaoo, B. Prasad, R. Singh, P.K. Mukhopadhyay, B.N. Upadhyaya, Effect of laser fluence on signal sustainability and quantitative performance of fiber-optic LIBS for steel samples, Spectrochimica Acta Part B: Atomic Spectroscopy 235 (2026) 107362.